Hindawi
Mathematical Problems in Engineering
Volume 2020, Article ID 8764349, 17 pages
https://doi.org/10.1155/2020/8764349

Research Article

Analytical, Numerical, and Experimental Investigations on Transverse Bending Responses of CFRP Square Tube Filled with Aluminum Foam

Dejun Yin,[1] **Jian Zheng**,[1] **Chao Xiong**,[1] **Junhui Yin**,[1] **Baochen Li**,[2] **Huiyong Deng**,[1] **and Xiujie Zhu**[1]

[1]*Department of Artillery Engineering, Shijiazhuang Campus, Army Engineering University, Shijiazhuang City 050003, China*
[2]*Offices of Research and Development, Army Engineering University, Nanjing City 210000, China*

Correspondence should be addressed to Jian Zheng; zj3373775258@163.com and Chao Xiong; xiongchao@tsinghua.org.cn

Received 5 November 2019; Revised 11 December 2019; Accepted 2 January 2020; Published 11 May 2020

Academic Editor: A. M. Bastos Pereira

In order to explore the transverse bending responses of carbon fiber-reinforced polymer (CFRP) square tubes filled with aluminum foam, the three-point bending tests were carried out on an INSTRON machine, the full-field deformation measurement was performed using a 3D-DIC test system, the numerical model was established by ABAQUS/Explicit, and the bending stiffness was calculated by the improved analytical model based on shear-deformable beam theory. The discrepancies of experimental data, numerical results, and analytical predictions were acceptable, which were within 5%. The failure modes and mechanical properties of the filled tubes were experimentally captured and numerically predicted. Due to the filling effect of aluminum foam, the ultimate load, bending stiffness, and energy absorption of the filled CFRP square tubes increased, comparing to those of the hollow CFRP square tubes. With the increase of the aluminum foam density, the ultimate load, bending stiffness, and energy absorption of the filled tubes increased, while the specific ultimate load, specific bending stiffness, and specific energy absorption decreased.

1. Introduction

With the increasing demands on safety and crashworthiness of vehicle transportation, a large number of researches have been carried out on the energy absorption capacity, crash response, and progressive collapse mode of energy absorbing devices from experimental and numerical points of view [1–4]. The load-carrying capacity and energy absorption capacity of automobile structural components are the key issues in lightweight design of vehicle body structure [5–7]. Thin-walled tubular structure as a common structural form in engineering has widely been used in automobile structural parts [8–10]. So far, there have been considerable published studies available regarding the crashworthiness of various thin-walled structures, such as double hat shaped tubes [11, 12], star-shaped tubes [13], octagonal tubes [14], corrugated tubes [15, 16], double section bitubular thin-walled structures [17], and conical tubes [18].

The previous articles have shown that the mechanical properties of hollow tubes can be improved by inserting the lightweight materials such as wood, rubber, honeycomb, or foam as filler materials inside the empty tubes [19–24]. For example, Movahedi and Linul [25] explored the uniaxial compression properties of thin-walled steel tubes filled with closed-cell aluminum foam; and they concluded that inserting aluminum foam as filler materials improved the energy absorption by 23%. Mohsenizadeh and Ahmad [26] studied the crushing characteristics and energy absorption of thin-walled aluminum tubes filled with auxetic foam under the axial loading condition. Results showed that

increasing the auxeticity level of foam filler enhanced crashworthiness performance of foam-filled structures under both quasi-static and dynamic loading conditions. Asavavisithchai et al. [27] investigated the effect of tube length on the bucking mode and energy absorption of aluminum foam-filled tubes under quasi-static axial loading; and they found that the energy absorption of foam-filled tube was higher than the sum of the absorbed energy of foam and hollow tube individually due to interaction effect.

Carbon fiber-reinforced plastic (CFRP) materials have widely been used in aeronautic and automotive structures attributable to the advantages of specific strength, modulus, and energy absorption over the traditional metallic materials [28–31]. A large number of published studies focused on the crushing responses and energy absorption capability of CFRP structures. Mamalis et al. [32] observed different brittle failure modes of CFRP square tubes under quasi-static axial compression loading; and they analyzed the influence of geometric characteristics on compression responses and collapse modes. Othman et al. [33] investigated the crushing behavior of polyurethane (PU) foam-filled pultruded composite square tubes under quasi-static axial and oblique loading. Results indicated that PU foam enhanced the absorbed energies. Liu et al. [34] discussed the mechanical behavior and failure mechanism of CFRP square tubes filled with aluminum honeycomb under quasi-static axial compression; and they found that the peak load and absorbed energy were increased while the specific energy absorption decreased with the decrease of the aluminum honeycomb cell width. Sun et al. [35] performed axial compression tests to study the crashworthiness of empty/aluminum foam/honeycomb-filled CFRP tubes. The results showed that the specific energy absorption of filled CFRP tubes were slightly lower than the empty counterparts but far better than those of all metal specimens.

Some studies on the analytical model of CFRP structures were conducted. Mai et al. [36] optimized the design of box-section sandwich beams under three-point bending load by establishing an analytical model considering shear deformation and studied the relationship between mass and stiffness. Vo and Lee [37–39] established the tensile-bending-shear-torsion coupling deformation analysis model of thin-walled composite box beams using the first-order shear deformation theory, but they ignored the elastic coupling effect in calculating the equivalent stiffness. Geuchy and Hoa [40] calculated the equivalent bending stiffness of thick-walled composite tubes with balanced antisymmetric ply based on the stress-strain field of composite tubes under pure bending. Shadmehri et al. [41] deduced the equivalent constitutive equation of composite tubes based on the displacement field of composite tubes and three-dimensional laminate theory which was applicable to any cross-sectional shape, but the calculation of the equivalent stiffness coefficient was complicated.

Generally speaking, the foam density of filler is the most obvious factor affecting mechanical property and bending response behavior of a foam-filled tube [33, 42]. According to the existing literatures, the influence of aluminum foam filler on the bending characteristics of CFRP square tubes is relatively limited by the combination of experimental investigation, numerical model, and analytical model. In order to better understanding of crashworthiness of CFRP tubes, the experimental investigation into the aluminum foam, hollow CFRP square tube, and CFRP square tube filled with aluminum foam will be performed under the quasi-static three-point transverse bending condition in this paper, and the full-field strain of the CFRP tubes will be characterized by the three-dimensional digital image correlation (3D-DIC) test system. The 3D finite element model of composite laminates progressive damage analysis will be established based on continuum damage mechanism by ABAQUS/Explicit to investigate the bending behavior and failure modes of CFRP structure. The analytical model of the CFRP square tube will be developed based on shear-deformable beam theory considering nonclassical effects such as lateral shear deformation, three-dimensional strain, and warping. The load-deflection curves, full-field strain distribution characteristics, damage evolution process, and filling effect aluminum foam of hollow and aluminum foam-filled CFRP tubes will be evaluated and discussed in detail by comparing of experimental data, numerical results, and analytical predictions.

2. Experimental Methods

2.1. Characteristics Criteria. Several key crashworthiness parameters are quantified to compare the bending performance of the tested structures. P_u is the ultimate load; $P_{u/m} = P_u/m$ is the ratio of ultimate load P_u to total mass; K_b is the bending stiffness; and $K_{b/m} = K_b/m$ is the ratio of bending stiffness to total mass. P_u can be determined by the measured load-deflection curves, and the bending stiffness K_b of specimens can be determined using the following formula [40]:

$$K_b = \frac{P_u L H}{8\varepsilon}, \tag{1}$$

where L is the distance between the two supports, H is the height of the specimen, and ε is the midspan strain.

Mean crushing load (P_{mean}), energy absorption (EA), and specific energy absorption (SEA) can be expressed as follows:

$$\begin{aligned} P_{\text{mean}} &= \frac{1}{l}\int_0^l P\mathrm{d}l, \\ \text{EA} &= \int_0^l P\mathrm{d}l, \\ \text{SEA} &= \frac{\int_0^l P\mathrm{d}l}{m}, \end{aligned} \tag{2}$$

where P is the instantaneous bending force, l is the bending deflection, and m is the mass of the specimen.

2.2. Sample Preparation. The unidirectional carbon fiber T300/QY8911 prepreg with around 58% of fiber volume fraction was chosen to fabricate the square tubes. The circumferential uniform stiffness (CUS) method with uniform

circumferential stiffness was adopted in the laying mode; the thickness of a single ply was taken as 0.125 mm, the total number of layers was 12, and the order of the layup was $[0/90]_6$. The CFRP square tubes were fabricated by the autoclave techniques. The autoclave system was heated up to around 120°C, and a pressure of 1.2 MPa was applied on the preforms. Then the fabricated tubes were cured for about 120 min to obtain the best strength and hardness. Finally, the cured tubes (1000 mm) were cut into the required length of specimens (160 mm) by the cutting machine; the two ends of specimens were machined to flat, without chamfering trigger features.

Closed-cell aluminum foam was prepared by the melt foaming method. The raw materials needed were pure Al, pure Mg, Ca particles (tackifier), and TiH_2 (foaming agent). The preparation process is illustrated in Figure 1(a), and the photograph of the prepared aluminum foam with the average density of 0.5 g/cm^3 is shown in Figure 1(b). The specimens were machined by the high-speed wire electrical-discharge machining (HSWEDM) to reduce the damage to the pore wall of aluminum foam specimens. Finally, the hollow CFRP square tube and aluminum foam were bonded with epoxy resin (E-44).

2.3. Geometry of Specimens. In this study, the three-point bending tests of pure aluminum foam, hollow CFRP square tube, and CFRP square tube filled with aluminum foam were carried out to investigate the bending characteristics. In order to ensure the accuracy of the test results, each test configuration was repeated with three specimens. The length and cross-sectional dimensions of the specimens are shown in Figure 2. The detailed information and characteristics of the tested specimens are summarized in Table 1.

2.4. Testing Procedure. The quasi-static three-point bending tests were carried out at room temperature in an INSTRON 5982 electronic universal testing machine (INSTRON, U.S.) with a loading capacity of 100 kN, as shown in Figure 3(a). The specimens were loaded at a consistent rate of 2 mm/min with the crushing distance of 20 mm. The specimens were placed between the indenter and supports without any fixing device; the span between two supports was 130 mm, as shown in Figure 3(b). The load and displacement data of the specimens can be obtained directly through the automatic data acquisition system. The whole experiment process was recorded by using a digital camera (CANON, Japan), as shown in Figure 3(a).

The strain gauge was attached to the bottom of the midspan, and the real-time strain data acquisition was carried out by using DH8303 strain measurement system (DONGHUA, China). The full-field strain distribution of the tested specimens was characterized by using 3D digital image correlation (3D-DIC) test system (PMLAB, China), as shown in Figure 3. In order to improve the accuracy of the 3D-DIC system, speckle images were produced by artificial spraying, as shown in Figure 3(c). Detailed test methods can be found in the existing literatures [43, 44].

3. Numerical Model

3.1. Damage Initiation Criteria and Damage Evolution for CFRP. 2D Hashin failure criteria were used to control the damage behavior for CFRP. These criteria have taken into account the effect of stress components on different damage modes, which can distinguish the four failure modes of fiber tensile, fiber compression, matrix tensile, and matrix compression. The initiation criteria have the following general forms [45, 46]:

Fiber tension ($\sigma_{11} \geq 0$):

$$F_{ft} = \left(\frac{\sigma_{11}}{X_T}\right)^2 + \alpha\left(\frac{\sigma_{12}}{S_L}\right)^2 \geq 1. \tag{3}$$

Fiber compression ($\sigma_{11} < 0$):

$$F_{fc} = \left(\frac{\sigma_{11}}{X_C}\right)^2 \geq 1. \tag{4}$$

Matrix tension ($\sigma_{22} \geq 0$):

$$F_{mt} = \left(\frac{\sigma_{22}}{Y_T}\right)^2 + \alpha\left(\frac{\sigma_{12}}{S_L}\right)^2 \geq 1. \tag{5}$$

Matrix compression ($\sigma_{22} < 0$):

$$F_{mc} = \left(\frac{\sigma_{22}}{2S_T}\right)^2 + \left[\left(\frac{Y_C}{2S_T}\right)^2 - 1\right]\frac{\sigma_{22}}{Y_C} + \left(\frac{\sigma_{12}}{S_L}\right)^2 \geq 1, \tag{6}$$

where F_i ($i = ft, fc, mt, mc$) denote the damage parameters corresponding to the four failure modes; σ_{ij} are components of stress tensor; X_T and X_C denote the longitudinal tensile strength and compressive strength, respectively; Y_T and Y_C are the transverse tensile strength and compressive strength, respectively; and S_L and S_T are the longitudinal and transverse shear strength, respectively. The engineering elastic constants and damage strength values of CFRP are derived from the manufacturer, as shown in Table 2.

When damage occurs in a ply, the mechanical properties will decline to a certain extent. In this paper, a linear degradation model based on fracture toughness was used for stiffness attenuation, as shown in Figure 4, where $\delta_{0,i}$ ($i = ft, fc, mt, mc$) is the initial damage displacement, $\sigma_{0,i}$ is the initial damage equivalent stress, $\delta_{f,i}$ is the complete damage displacement, and d_i is the damage state variable. It can be seen from Figure 4 that the equivalent strain energy of CFRP in complete failure can be calculated as follows:

$$W_s = \frac{\sigma_{0,i}\delta_{f,i}}{2}. \tag{7}$$

Table 3 is the fracture energy parameter for CFRP used in the tested specimens [47]. When the CFRP fails completely, the equivalent strain energy W_s is equal to its fracture energy G_i^C. At this time, the complete damage displacement can be calculated as

$$\delta_{f,i} = \frac{2G_i^C}{\sigma_{0,i}}. \tag{8}$$

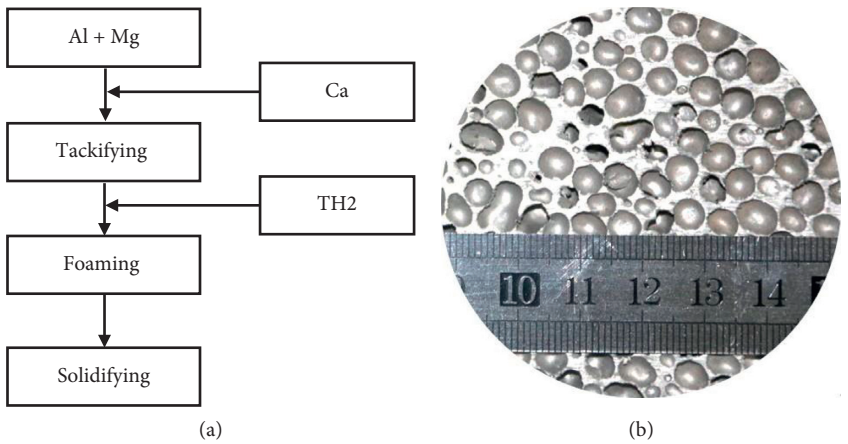

Figure 1: (a) Schematic diagram of fabrication process and (b) photograph of the prepared aluminum foam.

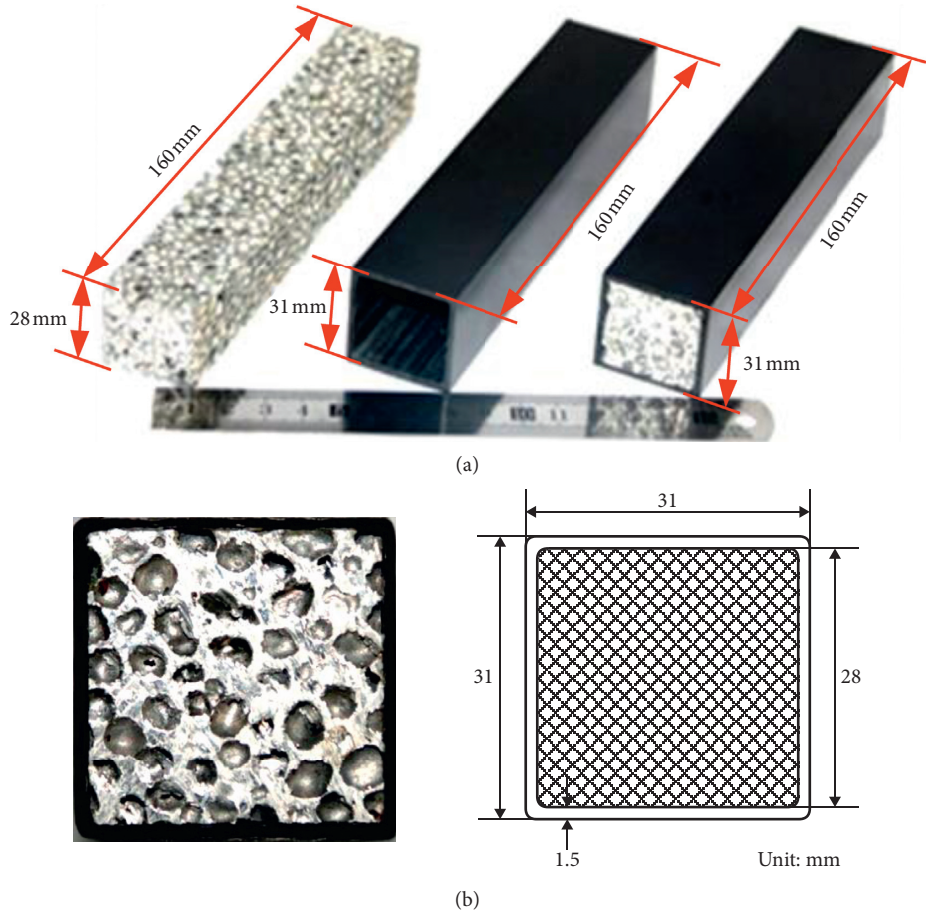

Figure 2: Schematic of (a) specimens in three-point bending test and (b) cross-sectional morphology and dimension of the CFRP square tube filled with aluminum foam.

The degradation degree of the mechanical properties of the material is characterized by the damage state variable d_i, which is expressed as

$$d_i = \frac{\delta_{f,i}\left(\delta_i - \delta_{0,i}\right)}{\delta_i\left(\delta_{f,i} - \delta_{0,i}\right)}. \tag{9}$$

The constitutive relation of composite monolayer during damage evolution is

$$\sigma = \mathbf{C}_d \varepsilon, \tag{10}$$

where $\mathbf{C}_d$ is the stiffness matrix considering the damage, and the calculation formula is

Table 1: Detailed information and bending characteristics of tested specimens under three-point bending condition.

Specimen	m (g)	P_u (N)	$P_{u/m}$ (N/g)	K_b (N·m^2)	$K_{b/m}$ ((N·m^2)/g)	EA (J)	SEA (J/g)
AF-1	63.3	1,329	21.0	9,388,954	148,325	9.9	0.16
AF-2	62.5	1,354	21.7	9,375,768	150,012	10.2	0.16
AF-3	61.8	1,313	21.2	9,369,894	151,616	9.6	0.16
Mean	62.5	1,332	21.3	9,378,205	150,001	9.9	0.16
HT-1	45.3	4,776	105.4	1,729,913,386	38,187,933	48.1	1.06
HT-2	42.8	4,590	107.2	1,727,398,192	40,359,771	45.7	1.07
HT-3	43.4	4,655	107.3	1,736,188,003	40,004,332	46.9	1.08
Mean	43.8	4,674	106.7	1,731,166,527	39,517,345	46.9	1.07
FT-1	107.3	7,867	73.3	1,772,478,686	16,518,907	97.9	0.91
FT-2	111.8	7,897	70.6	1,757,813,225	15,722,837	102.7	0.92
FT-3	108.4	7,932	73.2	1,789,928,727	16,512,258	97.6	0.90
Mean	109.2	7,899	72.3	1,773,406,879	16,251,334	99.4	0.91

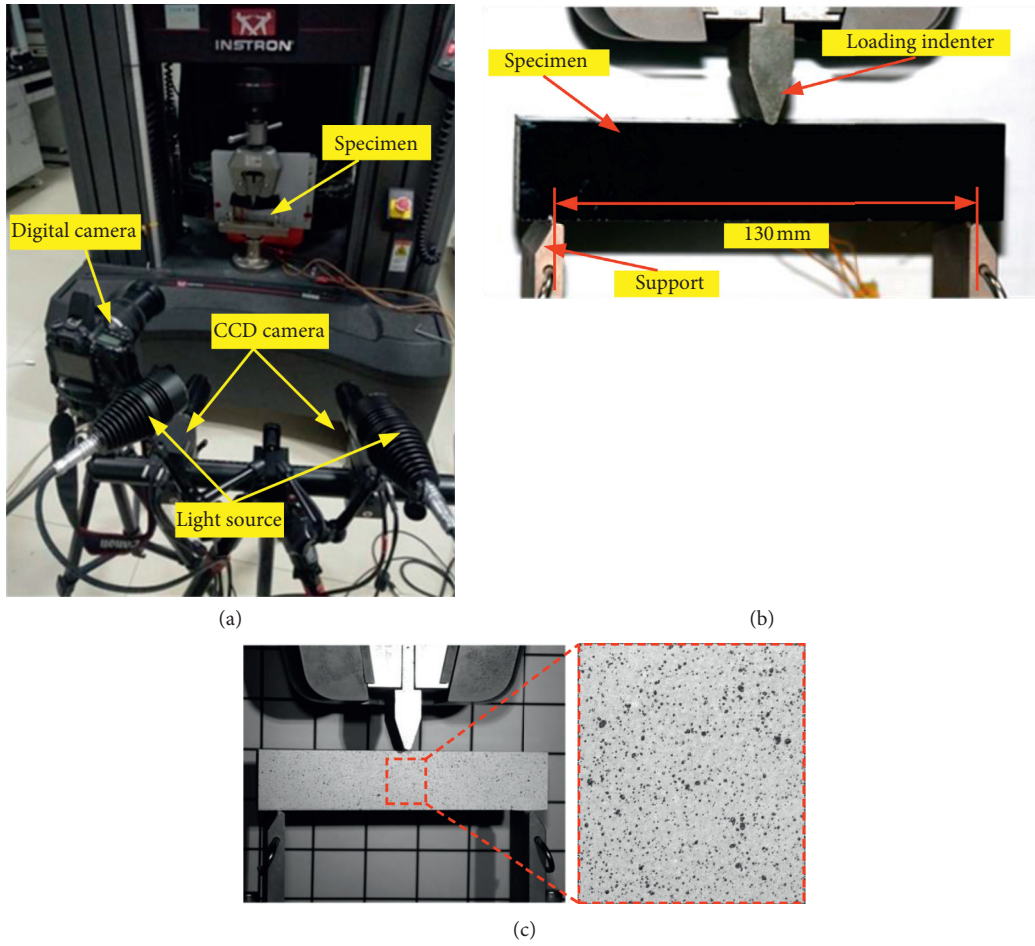

Figure 3: Test setups: (a) testing machine with 3D-DIC system, (b) testing machine with 3D-DIC system, and (c) specimen with speckle.

Table 2: Mechanical property of uniaxial laminates.

E_{11} (GPa)	$E_{22} = E_{33}$ (GPa)	$\nu_{12} = \nu_{13}$	ν_{23}	$G_{12} = G_{13}$ (GPa)	G_{23} (GPa)
135	8.8	0.33	0.33	4.47	3.0
X_T (MPa)	X_C (MPa)	Y_T (MPa)	Y_C (MPa)	$S_L = S_T$ (MPa)	ρ (g/cm^3)
1673	1160	68	210	112	1.58

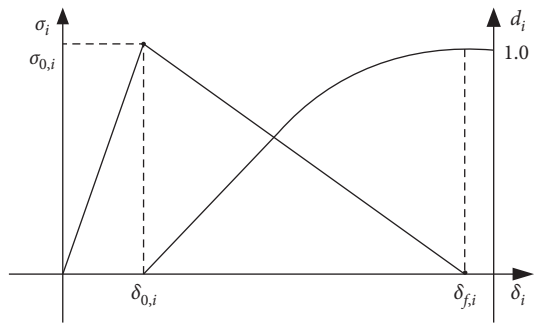

Figure 4: Linear degradation model in damaged composite laminate.

Table 3: Composite material fracture energy parameters [47].

G_{ft}^C (N/mm)	G_{fc}^C(N/mm	G_{mt}^C (N/mm)	G_{mc}^C (N/mm)
50.5	30.5	0.22	1.1

$$\mathbf{C}_d = \frac{1}{D}\begin{bmatrix} (1-d_f)E_1 & (1-d_f)(1-d_m)\nu_{21}E_1 & 0 \\ (1-d_f)(1-d_m)\nu_{21}E_1 & (1-d_m)E_2 & 0 \\ 0 & 0 & D(1-d_s)G_{12} \end{bmatrix}, \tag{11}$$

where $D = 1 - (1 - d_f)(1 - d_m)$ and d_f, d_m, and d_s are the state variables of fiber damage, matrix damage, and in-plane shear damage, respectively, which can be expressed as follows:

$$d_f = \begin{cases} d_{ft}, & \sigma_{11} \geq 0, \\ d_{fc}, & \sigma_{11} < 0, \end{cases}$$
$$d_m = \begin{cases} d_{mt}, & \sigma_{11} \geq 0, \\ d_{mc}, & \sigma_{11} < 0, \end{cases} \tag{12}$$
$$d_s = 1 - (1 - d_{ft})(1 - d_{fc})(1 - d_{mt})(1 - d_{mc}).$$

The relationship between the effective stress matrix and the real stress matrix is as follows:

$$\overline{\sigma} = \mathbf{M}\sigma, \tag{13}$$

where $\mathbf{M}$ is the damage coefficient matrix, which is calculated by the following formula:

$$\mathbf{M} = \begin{bmatrix} \frac{1}{1-d_f} & 0 & 0 \\ 0 & \frac{1}{1-d_m} & 0 \\ 0 & 0 & \frac{1}{1-d_s} \end{bmatrix}. \tag{14}$$

3.2. Elastoplastic Constitutive Model for Aluminum Foam. An ideal elastoplastic model was used for aluminum foam core materials, and the constitutive equation of aluminum foam considering density effect can be expressed by equation (15) [24, 48]. Figure 5 plots the stress-strain curves of aluminum foam with different densities [24]:

$$\sigma = 20.34\rho^{1.69}\frac{e^{94.58\rho^{0.08}\varepsilon} - 1}{1 + e^{94.41\rho^{0.08}\varepsilon}} + e^{12.34\rho - 10.55}\left[e^{(-8.6\rho + 14.68)\varepsilon} - 1\right]. \tag{15}$$

3.3. Mesh Generation and Boundary Conditions. In this paper, ABAQUS/Explicit was used to establish the numerical model of specimens under three-point bending condition. The CFRP square tube was cut into 12 layers along the thickness direction, and each layer was simulated by an SC8R continuous shell element with a thickness of 0.125 mm. COH3D8 interface element with zero thickness was arranged between layers to simulate the debonding damage, and COH3D8 interface element with a thickness of 0.01 mm was used to simulate the interfacial bonding between the CFRP square tube and aluminum foam [49, 50]. C3D8R three-dimensional stress element was used to simulate the aluminum foam core material. The indenter and two supports were defined as discrete rigid bodies. The two supports were defined as the clamped boundary condition, while the indenter could move vertically. A universal contact with a tangential friction coefficient of 0.1 and a normal "hard" contact [51] were established. MPC constraint was set

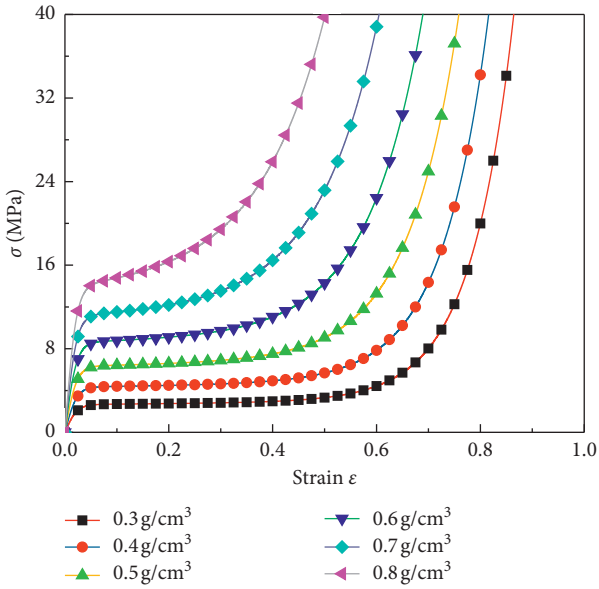

FIGURE 5: Stress-strain curves of aluminum foam with different densities.

between the indenter and the reference point, and the vertical displacement loading was applied at the reference point. The finite element models of CFRP square tube filled with aluminum foam is shown in Figure 6.

4. Analytical Model

4.1. Simplification of Constitutive Equation for CFRP Square Tube. In order to describe the deformation of the CFRP square tube, the Cartesian coordinate system (x, y, z) was used for the overall coordinates, and the coordinate origin was located at the centroid of the cross section; the curvilinear coordinate system (z, s, n) was used as the local coordinates, and the coordinate origin was located at the middle line of the cross section; n represents the normal direction of the plane line, and s is the tangential direction of the middle plane line, as shown in Figure 7.

The three-dimensional constitutive relation of any single layer for CFRP is as follows:

$$\begin{Bmatrix} \sigma_z \\ \sigma_s \\ \sigma_n \\ \tau_{sn} \\ \tau_{nz} \\ \tau_{sz} \end{Bmatrix}_k = \begin{bmatrix} \overline{C_{11}} & \overline{C_{12}} & \overline{C_{13}} & 0 & 0 & \overline{C_{16}} \\ \overline{C_{12}} & \overline{C_{22}} & \overline{C_{23}} & 0 & 0 & \overline{C_{26}} \\ \overline{C_{13}} & \overline{C_{23}} & \overline{C_{33}} & 0 & 0 & \overline{C_{36}} \\ 0 & 0 & 0 & \overline{C_{44}} & \overline{C_{45}} & 0 \\ 0 & 0 & 0 & \overline{C_{45}} & \overline{C_{55}} & 0 \\ \overline{C_{16}} & \overline{C_{26}} & \overline{C_{36}} & 0 & 0 & \overline{C_{66}} \end{bmatrix}_k \begin{Bmatrix} \varepsilon_z \\ \varepsilon_s \\ \varepsilon_n \\ \gamma_{sn} \\ \gamma_{nz} \\ \gamma_{sz} \end{Bmatrix}_k, \tag{16}$$

where $\overline{C_{ij}}$ represents the three-dimensional stiffness coefficient under the off-axis coordinate system.

The stress components out of the cross section (σ_n, σ_s, and τ_{sn}) were much smaller than the in-plane stress components (σ_z, τ_{nz}, and τ_{sz}), where it can be assumed that $\sigma_n = \sigma_s = \tau_{sn} = 0$. Therefore, equation (16) could be simplified as follows:

$$\begin{Bmatrix} \sigma_z \\ \tau_{sz} \\ \tau_{nz} \end{Bmatrix} = \begin{bmatrix} C_{11}^* & C_{12}^* & 0 \\ C_{12}^* & C_{22}^* & 0 \\ 0 & 0 & C_{33}^* \end{bmatrix} \begin{Bmatrix} \varepsilon_z \\ \gamma_{sz} \\ \gamma_{nz} \end{Bmatrix}. \tag{17}$$

The formulas for calculating the three-dimensional converted stiffness coefficient C_{ij}^* in equation (17) were as follows.

$\overline{Q_{ij}}$ represents the two-dimensional converted modulus component in the classical laminate theory:

$$\begin{cases} C_{11}^* = \overline{Q_{11}} - \dfrac{\overline{Q_{12}}^2}{\overline{Q_{22}}}, \\ C_{12}^* = \overline{Q_{16}} - \dfrac{\overline{Q_{12}Q_{26}}}{\overline{Q_{22}}}, \\ C_{22}^* = \overline{Q_{66}} - \dfrac{\overline{Q_{26}}^2}{\overline{Q_{22}}}, \\ C_{33}^* = \overline{Q_{55}} - \dfrac{\overline{Q_{45}}^2}{\overline{Q_{44}}}. \end{cases} \tag{18}$$

4.2. Calculation of Bending Stiffness of CFRP Square Tube Filled with Aluminum Foam. According to the shear-deformable beam theory [14–17], the equivalent stiffness matrix of the CFRP square tubes by using orthogonal lay was as follows:

$$\begin{Bmatrix} N_z \\ M_y \\ M_x \\ V_x \\ V_y \\ M_\omega \\ M_z \end{Bmatrix} = \begin{bmatrix} a_{11} & 0 & 0 & 0 & 0 & 0 & 0 \\ & a_{22} & 0 & 0 & 0 & 0 & 0 \\ & & a_{33} & 0 & 0 & 0 & 0 \\ & & & a_{44} & 0 & 0 & 0 \\ & & & & a_{55} & 0 & 0 \\ & & & & & a_{66} & 0 \\ sym & & & & & & a_{77} \end{bmatrix} \begin{Bmatrix} w_0' \\ \theta_y' \\ \theta_x' \\ u_0' + \theta_y \\ v_0' + \theta_x \\ \varphi'' \\ \varphi' \end{Bmatrix}, \tag{19}$$

where N_z is the axial force; M_x, M_y, and M_z are the bending moments around the x, y, and z axes, respectively; M_w is the bimoment generated by the torsional normal stress; V_x and V_y are the shear forces in the x and y directions, respectively; u, v, and w are the displacements along the coordinate axes x, y, and z, respectively; $\theta_x(z)$, $\theta_x(z)$, and $\varphi(z)$ are the rotation angles around the coordinate axes x, y, and z, respectively; and $u_0(z)$, $v_0(z)$, and $w_0(z)$ are the rigid body displacements in the three directions.

The bending stiffness (K_b) of the CFRP squares can be obtained:

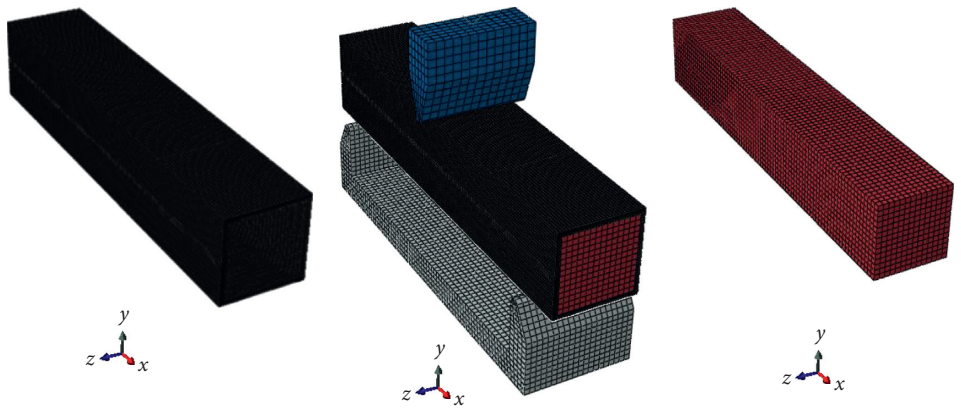

Figure 6: Finite element model of CFRP square tube filled with aluminum foam. (a) CFRP tube; (b) assembly; (c) aluminum foam.

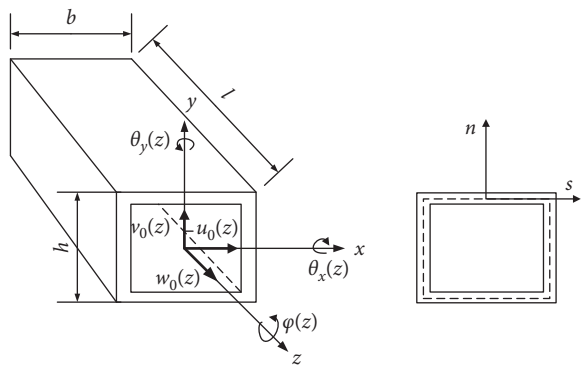

Figure 7: Coordinate system of the CFRP square tube.

$$K_b = \int_s \left[x^2 \left(A_{11} - \frac{A_{12}^2}{A_{22}} \right) + 2 \left(B_{11} - \frac{A_{12} B_{12}}{A_{22}} \right) x \sin\phi + \left(D_{11} - \frac{B_{12}^2}{A_{22}} \right) \sin^2\phi \right] \mathrm{d}s, \tag{20}$$

where ϕ is the angle between the n and the x directions and A_{ij}, B_{ij}, and D_{ij} are the in-plane stiffness coefficients, coupling stiffness coefficients, and bending stiffness coefficients in the classical laminate theory, respectively.

A_{ij}, B_{ij}, and D_{ij} can be obtained by the following calculation formula:

$$\int \overline{Q_{ij}} \left(1, n, n^2\right) \mathrm{d}n = \left(A_{ij}, B_{ij}, D_{ij}\right). \tag{21}$$

According to the superposition principle, the overall bending stiffness of the CFRP square tubes filled with aluminum foam is expressed as follows.

$\overline{Q_{ij}}$ can be obtained by the following calculation formula:

$$\begin{cases} \overline{Q_{ij}} = \overline{C_{ij}} - \dfrac{\overline{C_{i3} C_{3j}}}{\overline{C_{33}}}, & (i, j = 1, 2, 6), \\ \overline{Q_{ij}} = \overline{C_{ij}}, & (i, j = 4, 5), \end{cases} \tag{22}$$

where $\overline{C_{ij}}$ can be obtained by the following calculation formulas:

$$\begin{cases} \overline{C}_{11} = \cos^4\theta C_{11} + 2\cos^2\theta \sin^2\theta (C_{12} + 2C_{66}) + \sin^4\theta C_{22}, \\ \overline{C}_{12} = \cos^4\theta \sin^2\theta (C_{11} + C_{22} - 4C_{66}) + (\cos^4\theta + \sin^4\theta) C_{12}, \\ \overline{C}_{22} = \sin^4\theta C_{11} + 2\cos^2\theta \sin^2\theta (C_{12} + 2C_{66}) + \cos^4\theta C_{22}, \\ \overline{C}_{11} = \cos^4\theta C_{11} + 2\cos^2\theta \sin^2\theta (C_{12} + 2C_{66}) + \sin^4\theta C_{22}, \\ \overline{C}_{12} = \cos^4\theta \sin^2\theta (C_{11} + C_{22} - 4C_{66}) + (\cos^4\theta + \sin^4\theta) C_{12}, \\ \overline{C}_{22} = \sin^4\theta C_{11} + 2\cos^2\theta \sin^2\theta (C_{12} + 2C_{66}) + \cos^4\theta C_{22}, \\ \overline{C}_{16} = \cos\theta \sin\theta [\cos^2\theta C_{11} - \sin^2\theta C_{22} - (\cos^2\theta - \sin^2\theta)(C_{12} + 2C_{66})], \\ \overline{C}_{26} = \cos\theta \sin\theta [\sin^2\theta C_{22} - \cos^2\theta C_{11} + (\cos^2\theta - \sin^2\theta)(C_{12} + 2C_{66})], \\ \overline{C}_{66} = \cos^2\theta \sin^2\theta (C_{11} + C_{22} - 2C_{12}) + (\cos^2\theta - \sin^2\theta)^2 C_{66}, \end{cases} \tag{23}$$

where θ represents the fiber orientation angle of the CFRP square tube.

The bending stiffness (K_b) of the CFRP squares filled with aluminum foam can be obtained:

$$K_b = \int_s \left[x^2 \left(A_{11} - \frac{A_{12}^2}{A_{22}} \right) + 2 \left(B_{11} - \frac{A_{12} B_{12}}{A_{22}} \right) x \sin \phi + \left(D_{11} - \frac{B_{12}^2}{A_{22}} \right) \sin^2 \phi \right] ds + \frac{1}{12} E_f b_f^4, \tag{24}$$

where E_f is the elastic modulus of aluminum foam and b_f represents the side length of aluminum foam.

5. Results and Discussion

5.1. Load-Deflection Curve and Strain Distribution. Figure 8 displays the representative load-deflection curves for aluminum foam (AF-1), hollow CFRP square tube (HT-1), and CFRP square tube filled with aluminum foam (FT-1) in three-point bending tests. All the curves can be divided into two distinct stages, known as the initial elastic bending and bending collapse stages, respectively. Taking the curve of AF-1 (blue curve in Figure 8) as an example, in the elastic bending stage, the bending load increased until it reached the peak value of 1 329 N at the deflection of 2.75 mm (point A_1) and then dropped gradually with the increase of the deflection until the specimen failed completely. The curve of HT-1 (red curve in Figure 8) was somewhat different from the curve of AF-1. The bending load reached a peak value of 4 776 N at the deflection of 1.88 mm (point H_1), then fluctuated after this peak value, and finally dramatically decreased to a lower plateau level. The load-deflection curve of FT-1 (black curve in Figure 8) was similar to that of HT-1 at the initial elastic bending stage. When the deflection was 2.21 mm, the load reached the first peak value of 7 426 N (point F_1). The difference was that when the bending deflection of FH-1 reached 7.44 mm, the bending load rose again due to the mutual coupling effect of the side wall of the CFRP square tube and aluminum foam; then the bending load decreased rapidly and finally maintained on a higher plateau level.

Comparing the curves of HT-1 and FT-1, it is clear that FT-1 was always above HT-1, which revealed that the CFRP square tube filled with aluminum foam had better load-carrying capacity and energy absorption efficiency than those of hollow CFRP square tube. From Figure 8 and Table 1, it is clear that the load-carrying capacity of aluminum foam was very low, and the peak value was less than 2 000 N, which was much lower than that of CFRP square tube. When the aluminum foam was filled into the CFRP square tube, the peak load (P_u) and energy absorption (EA) of the filled CFRP square tube can be significantly increased. The results indicated that after filling the CFRP square tube with aluminum foam, there was a strong and effective interaction during the bending test, which can improve the bending mechanical properties of the CFRP square tube. It is interesting to notice that although aluminum foam was a kind of weak and lightweight filling material, it was beneficial to improve the load-carrying capacity and energy absorption of the whole structure.

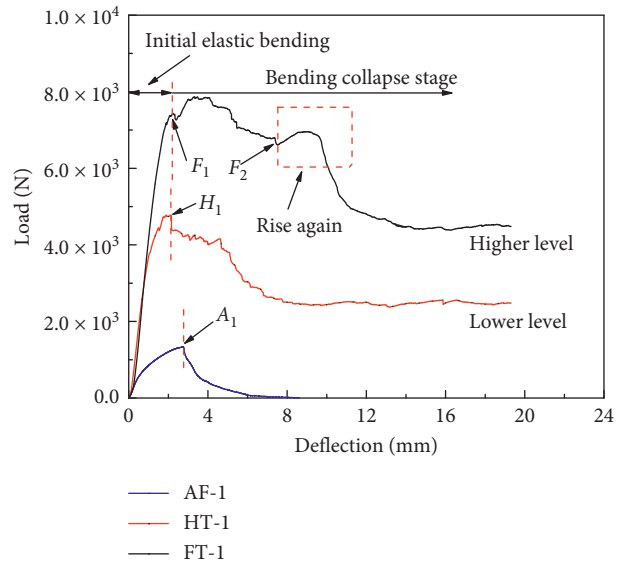

Figure 8: Typical load-deflection curves in transverse three-point bending tests.

The full-field strain distribution of HT-3 monitored at the load of 2 000 N was compared with the simulation results, as shown in Figure 9. The positive strain in the X direction ε_{xx} (along the axis of the CFRP square tube) was relatively small, and the trend of symmetry distribution was obvious, as shown in Figures 9(a) and 9(b); the shear strain ε_{xy} had better antisymmetry distribution, as shown in Figures 9(c) and 9(d); the positive strain in the Y direction ε_{yy} (along the vertical axis of the CFRP square tube) had better symmetry distribution, as shown in Figures 9(e) and 9(f). From the full-field strain distribution, it can be seen that strain concentration existed in the position of the indenter and supports. In addition, due to the anisotropy of CFRP, the strain distribution in the full-field of CFRP square tube was obviously different from that of the typical three-point bending. From Figure 9, it can be seen that the strain distribution by FEM was in good agreement with the strain distribution trend and strain value calculated by 3D-DIC, and the difference near the indenter and supports was large due to the "singularity."

5.2. Failure Mechanism. Figure 10 shows the typical failure progress of the aluminum foam (AF-1), hollow CFRP square tube (HT-1), and CFRP square tube filled with aluminum foam (FT-1) under different bending deflections (d). The typical damage characteristics of the aluminum foam were that the cracks gradually propagated from the bottom surface (tension surface) to upper surface (compression surface), the cell layers of aluminum foam squeezed to each other on the upper surface, and the cell layers stretched on the bottom surface, as shown in Figure 10(a). This is because the tensile strength of the aluminum foam cells is lower than that of the compression resistance.

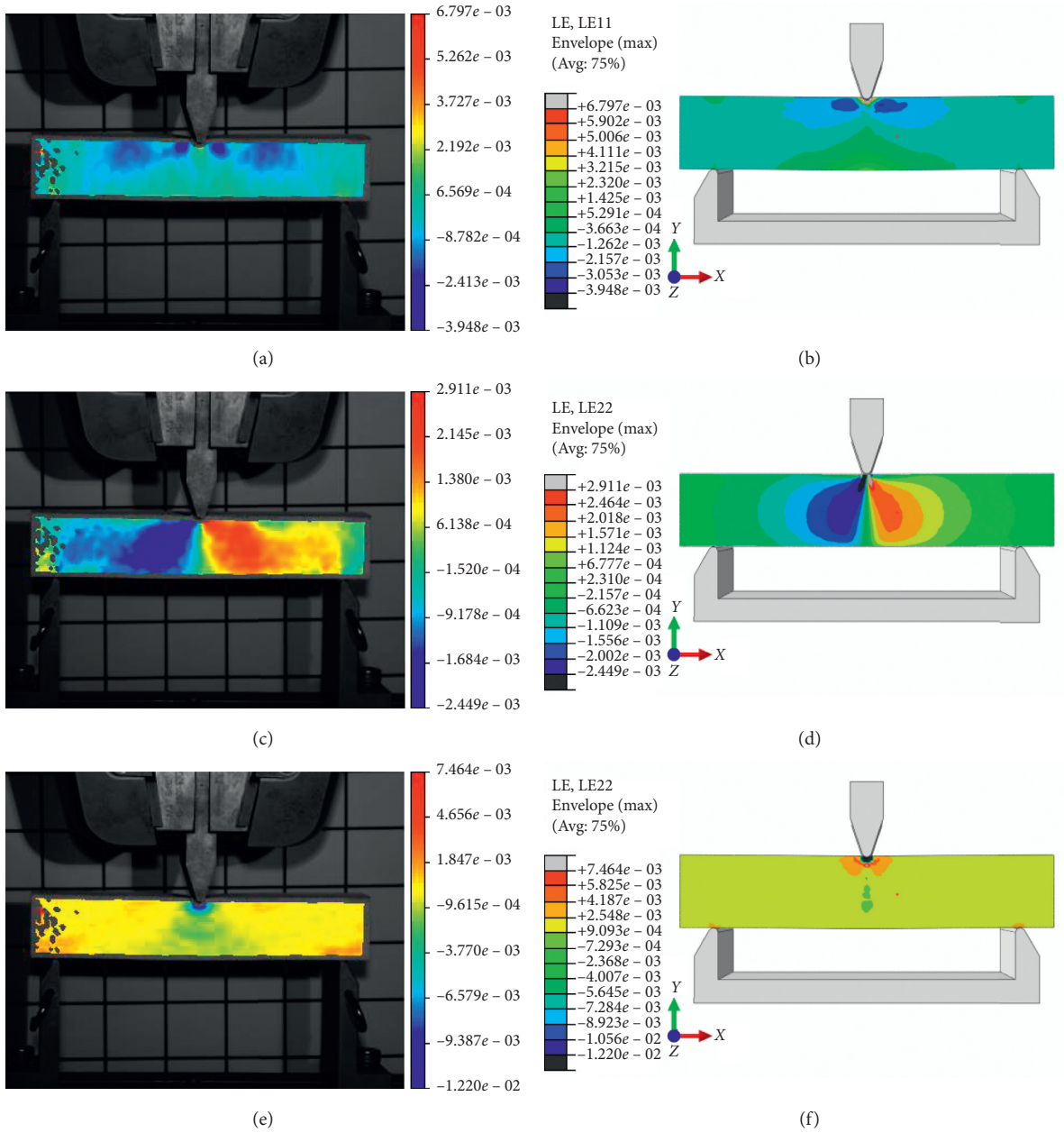

Figure 9: Full-field strain distribution of the specimen (HT-3) under the load of 2 000 N obtained by 3D-DIC and FEM: (a) ε_{xx} (3D-DIC), (b) ε_{xx} (FEM), (c) ε_{xy} (3D-DIC), (d) ε_{xy} (FEM), (e) ε_{yy} (3D-DIC), and (f) ε_{yy} (FEM).

Figure 10(b) reveals the damage evolution of hollow CFRP square tube (HT-1), including the indentation, buckling, plastic hinges, and bulging deformation. It should be noted that HT-1 developed plastic hinges with the increase of bending deflection, which allowed large deformation without reaching failure [52]. The top wall of the CFRP square tube was bent by compression and the bottom wall was bent by tension. There was a great stress concentration in the contact region between the indenter and the top wall, and then a large number of microcracks were sprouted at the top corner, resulting in the damage of resin compression and fiber fracture at the corner. Due to the combined effect of the extrusion by the indenter and the shear stress of the side wall of the CFRP square tube, the top corner begun to be crushed. With the further increase of deflection, the cracks propagated gradually from the top corner to the bottom corner along the direction perpendicular to the tube axis, and eventually the lateral wall of the CFRP square tube underwent out-of-plane bulging deformation. Because the compressive strength of CFRP was generally significantly lower than the tensile strength, the damage first occurred at the top wall of CFRP square tube and gradually extended to the bottom wall. The damage evolution process of CFRP square tube studied in this paper is consistent with the results in other literatures [11, 53].

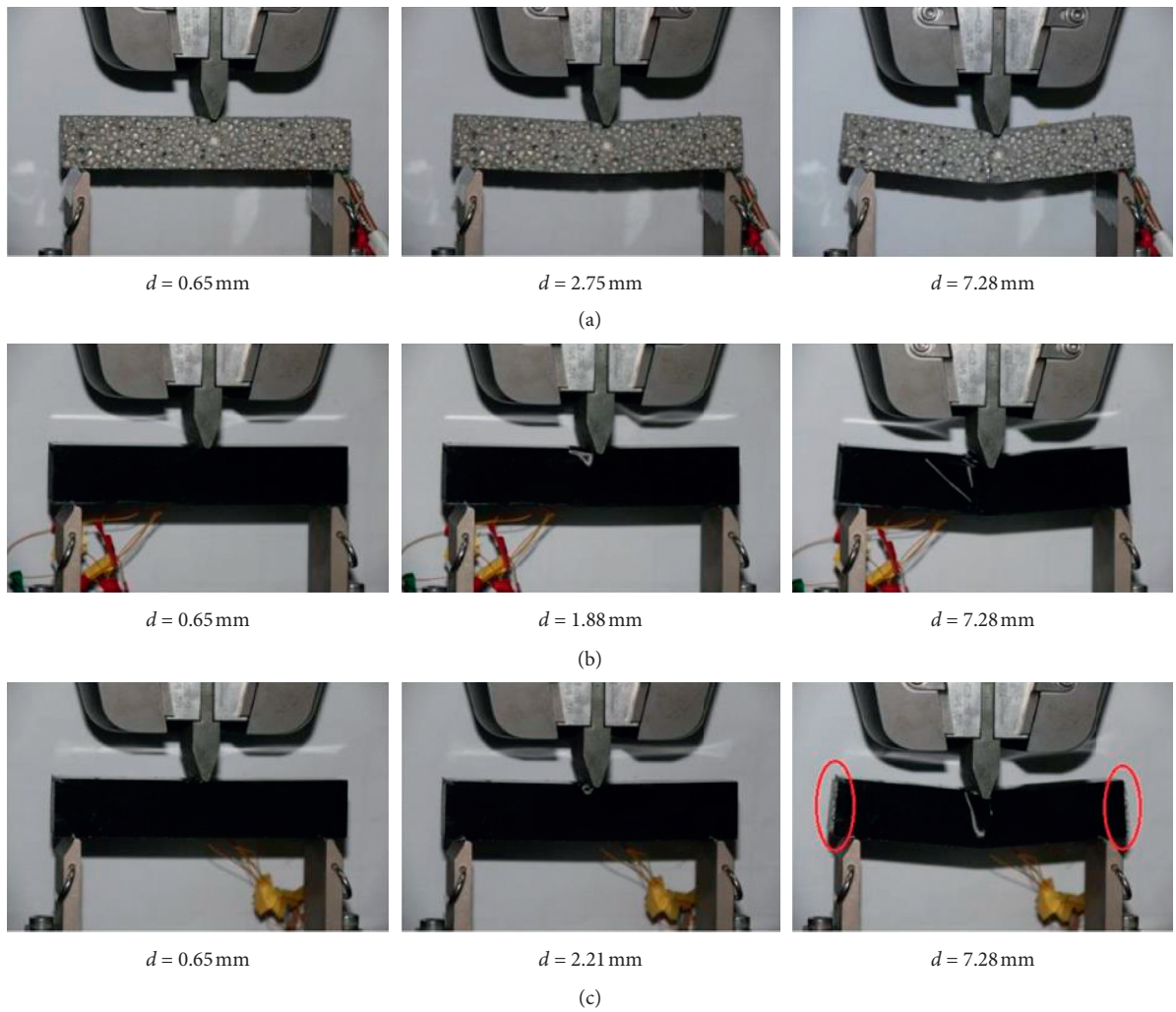

Figure 10: Failure process of the tested specimens under three-point bending load: (a) aluminum foam (AF-1), (b) hollow CFRP square tube (HT-2), and (c) CFRP square tube filled with aluminum foam.

The CFRP square tube filled with aluminum foam (FT-1 in Figure 10(c)) is displayed a more complex damage evolution process, including the indentation, buckling, plastic hinges, shear interaction, core failure, and bulging deformation. The failure mechanism of the outer CFRP square tube (FT-1) was similar to that of the hollow CFRP square tube (HT-1) as abovementioned. Due to the restriction of the CFRP square tube, the aluminum foam core near the indenter has not taken obvious local deformation. Because the interfacial bonding between the CFRP square tube and the aluminum foam core was destroyed after bending deformation, a narrow gap was observed with the increase of bending deflection, which allowed the sliding between the aluminum foam core and the CFRP square tube, especially at the two ends of the specimen, as shown in the areas of the circles in Figure 10(c).

Figure 11 shows four failure modes (i.e., fiber tensile, fiber compression, matrix tensile, and matrix compression) for the CFRP square tube filled with aluminum foam obtained by FEM when the load reached the ultimate load. As can be seen, the local deformation and indentation of the outer CFRP square tube begun to occur with the increase of bending deflection, and the stress concentration at the contact regions of the indenter and two supports were the most serious.

Figure 12 displays the stress clouds of outer CFRP square tube and inner aluminum foam at different bending loads (F) and deflections (d). After the ultimate load, the region of the top wall near the indenter begun to collapse, and the regions of the side walls near the indenter underwent out-of-plane bulging deformation with the increase of bending deflection. It is observed that the more red shade regions indicated a more severe deformation and stress concentration, and part of the failure element was removed. The aluminum foam core underwent overall bending deformation and local plastic deformation. The outer CFRP square tube and inner aluminum foam were degummed and misaligned caused by the inconsistent deformation of the external and internal structures.

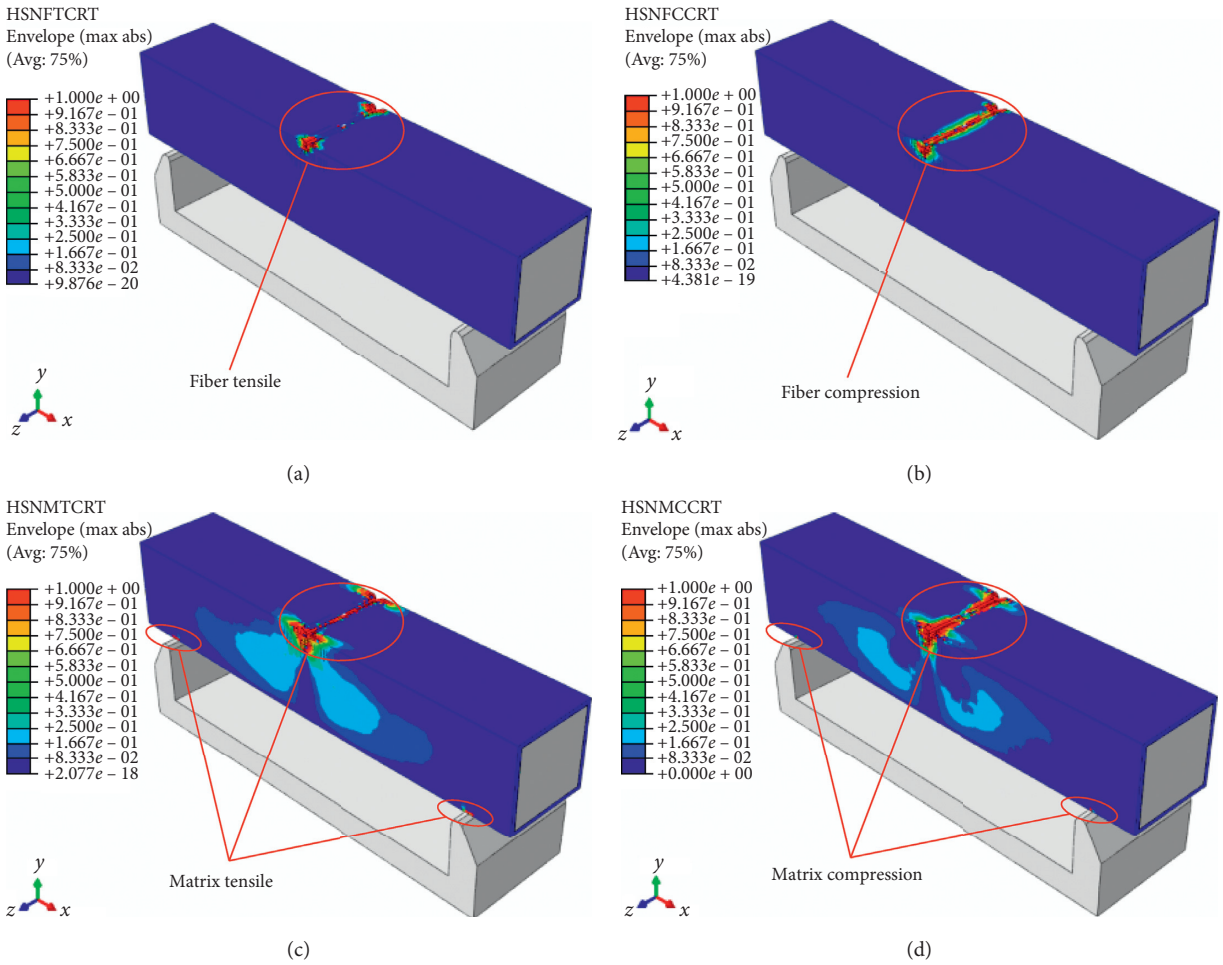

Figure 11: Failure modes of CFRP square tube filled with aluminum foam: (a) fiber tensile, (b) fiber compression, (c) matrix tensile, and (d) matrix compression.

5.3. Effect of Aluminum Foam Filler. The ultimate load (P_u) and bending stiffness (K_b) of the CFRP square tubes filled with aluminum foam were calculated by the numerical model and analytical model, respectively, and compared with the experimental results, as shown in Table 4. The average error of ultimate load (P_u) between the experimental values and calculated values by the numerical model was 4.81%, which proved the validity of the finite element model. The average error of bending stiffness (K_b) between the experimental values and calculated values by the analytical model was 4.47%, which can meet the accuracy requirement of the engineering application.

Table 1 and Figure 13 reveal the comparison of the load bearing, stiffness performance, and energy absorption characteristics between aluminum foam, hollow CFRP square tube, and CFRP square tube filled with aluminum foam. It can be seen that the ultimate load (P_u), bending stiffness (K_b), and energy absorption (EA) of the pure aluminum foam was only 1 332 N, 9 378 205 N·m^2, and 9.9 J, respectively; however, P_u, K_b, and EA of the CFRP square tubes filled with aluminum foam reached 7 899 N, 1 773 406 879 N·m^2, and 99.4 J increasing by approximate 69.0%, 2.4%, and 111.9% comparing to those of the hollow CFRP square tubes due to the effect of aluminum foam filler. Besides, the specific ultimate load ($P_{u/m}$), specific bending stiffness ($K_{b/m}$), and specific energy absorption (SEA) of the CFRP square tubes filled with aluminum (72.3 N/g, 16,251,334 (N·m^2)/g, and 0.91 J/g, respectively) slightly decreased by about 32.2 %, 58.9%, and 15.0%, comparing to those of the hollow CFRP square tubes (106.7 N/g, 39,517,345 (N·m^2)/g, and 1.07 J/g, respectively).

Other studies listed in Table 5 have comprehensively compared the bending behavior of the filled CFRP square tube with some traditional thin-walled structures. Liu et al. [53] carried out bending tests on empty CFRP square tubes and CFRP square tubes filled with aluminum honeycomb, and they found the EA of the filled CFRP tubes was 32.6% higher than hollow CFRP tubes. Aluminum tubes, as a kind of traditional thin-walled structures with excellent performance, have received extensive attentions. Shojaeifard et al. [54] performed experiments and numerical simulations to study the bending behavior of empty and foam-filled aluminum tubes with different cross sections (elliptic, square, and circular), and they found the EA of the elliptic, square, and circular foam-filled tubes was 22.5%, 17.0%, and 38.2% higher than empty aluminum tubes, respectively. The

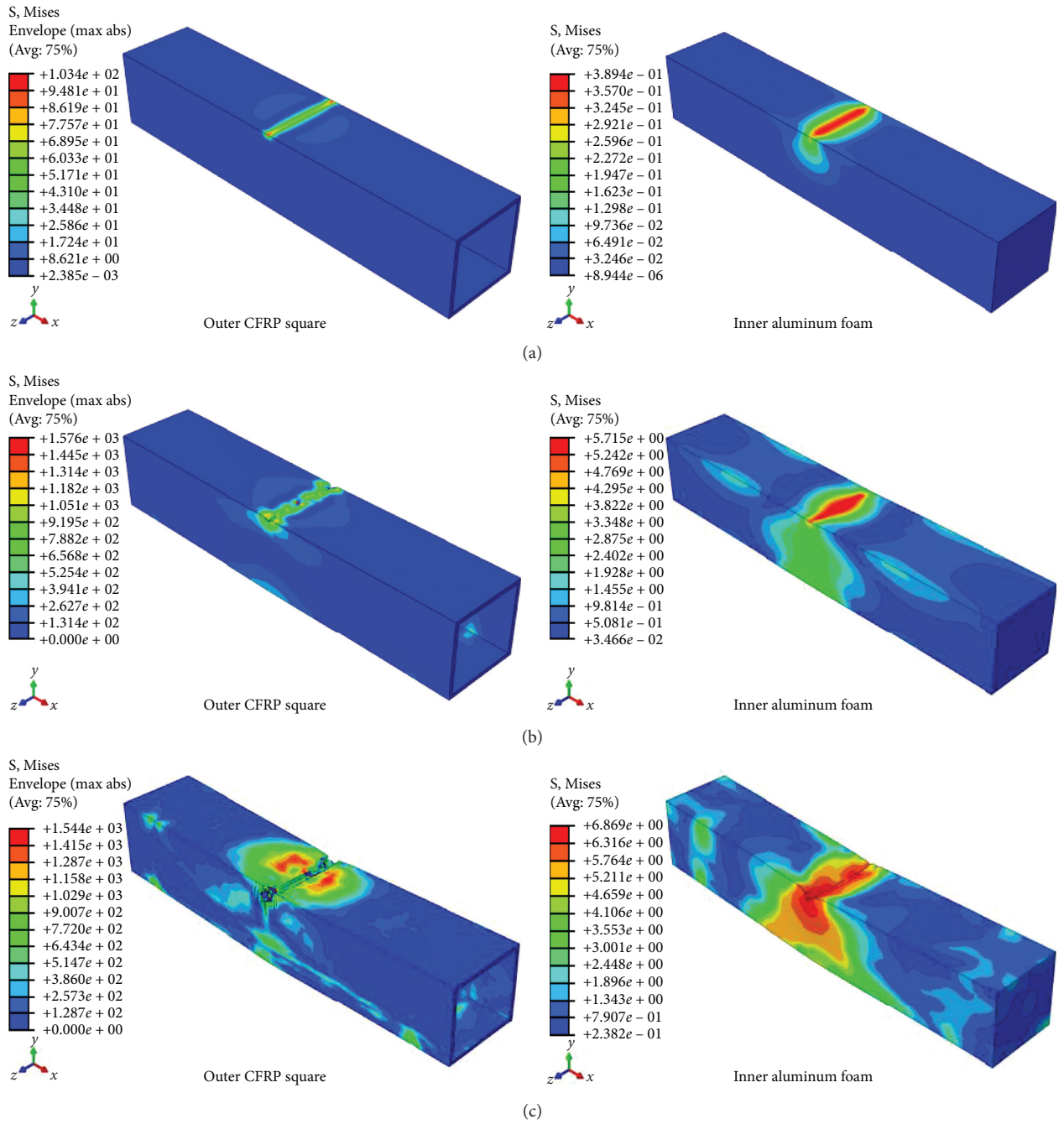

FIGURE 12: Stress clouds of the CFRP square tube filled with aluminum foam under three-point bending failure process: (a) $F = 3\ 297$ N, $d = 0.65$ mm; (b) $F = 7\ 379$ N, $d = 2.08$ mm; (c) $F = 6\ 370$ N, $d = 7.28$ mm.

comparison results indicated that although aluminum foam was rather weak as a kind of a lightweight filler material, it can effectively improve the energy absorption of the filled structure under bending load.

It was assumed that the cross-sectional geometric dimensions of the CFRP square tube filled with aluminum foam and the ply of CFRP square tubes remained unchanged. The variation of the mechanical properties of CFRP square tubes filled with aluminum foam with different densities was analyzed by the finite element model and analytical model, as shown in Figure 14. It is evident that the ultimate load (P_u), bending stiffness (K_b), and energy absorption (EA) increased with the increase of the density of aluminum foam; however, the specific ultimate load ($P_{u/m}$), specific bending stiffness ($K_{b/m}$), and specific energy absorption (SEA) decreased with the increase of the density of aluminum foam. This is because very high density of aluminum foam filler may cause undesirable crushing characteristics such as overall Euler buckling, premature tensile fracture, and low weight efficiency which were greatly reducing the energy absorption capability of filled structures [18, 27]. Therefore, the use of aluminum foam with low

Table 4: Performance parameter comparison of experimental results with the numerical model and analytical model calculation data for the CFRP square tubes filled with aluminum foam.

Performance parameter	Experiment	Numerical model	Analytical model	Error (%)
Ultimate load (N)	7 899	8 298	—	4.80
Bending stiffness (N·m^2)	1 773 406 879	—	1 856 387 396	4.47

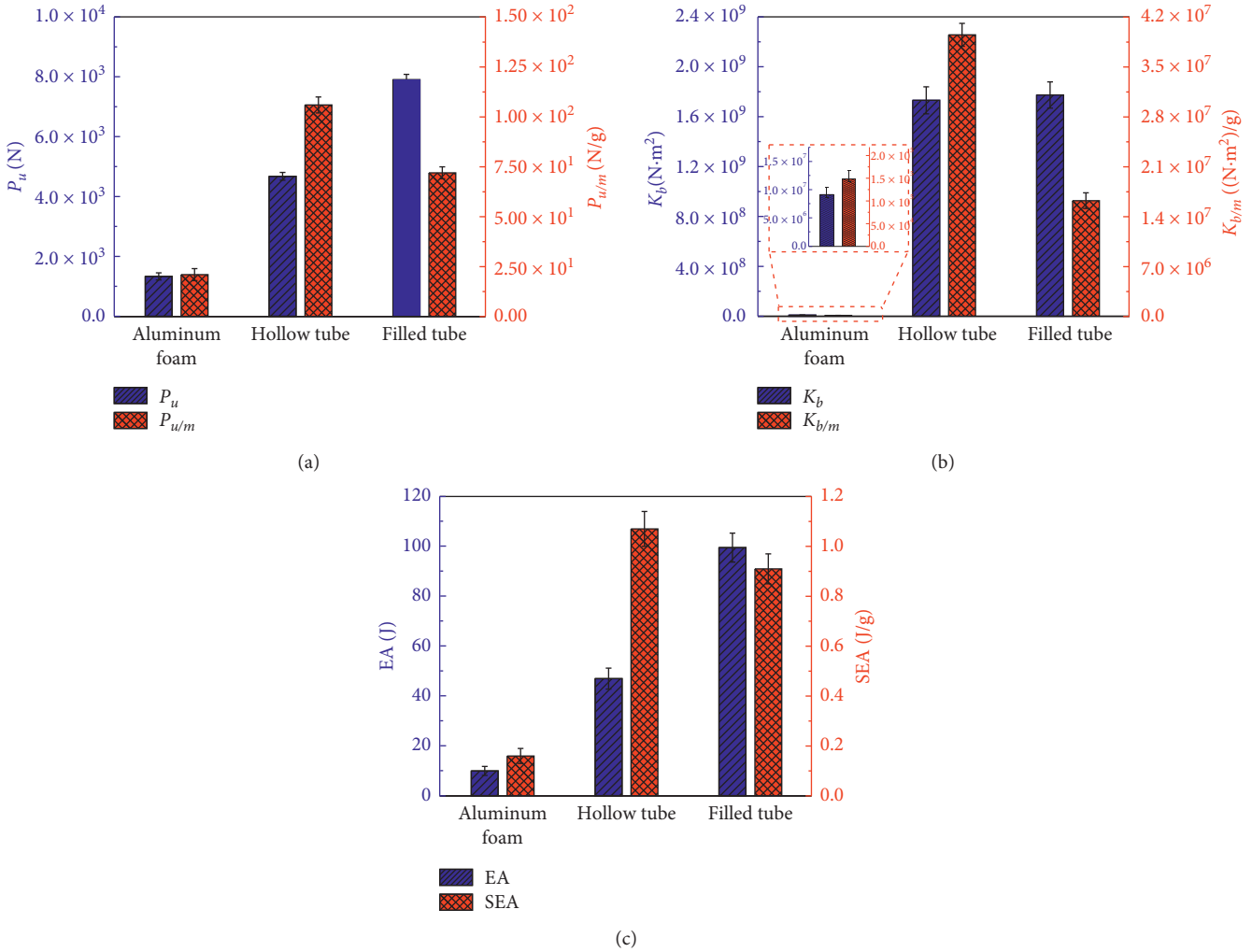

Figure 13: Comparison of the load bearing, stiffness performance, and energy absorption characteristics between aluminum foam, hollow CFRP square tube, and CFRP square tube filled with aluminum foam: (a) ultimate load (P_u) and specific ultimate load ($P_{u/m}$), (b) bending stiffness (K_b) and specific bending stiffness ($K_{b/m}$), and (c) energy absorption (EA) and specific energy absorption (SEA).

Table 5: Comprehensively compare the bending behavior of the filled CFRP square tube with some traditional thin-walled structures.

Tube type	Filler	EA (J)	Increase (%)	Reference
CFRP square tube	Hollow	46.9	112.0	This study
	Aluminum foam	99.4		
CFRP square tube	Hollow	177.3	32.6	Liu et al. [53]
	Aluminum honeycomb	235.2		
Elliptic aluminum	Hollow	155.3	22.5	
	Aluminum foam	190.2		
Square aluminum	Hollow	118.0	17.0	Shojaeifard et al. [54]
	Aluminum foam	138.1		
Circular aluminum	Hollow	117.3	38.2	
	Aluminum foam	162.2		

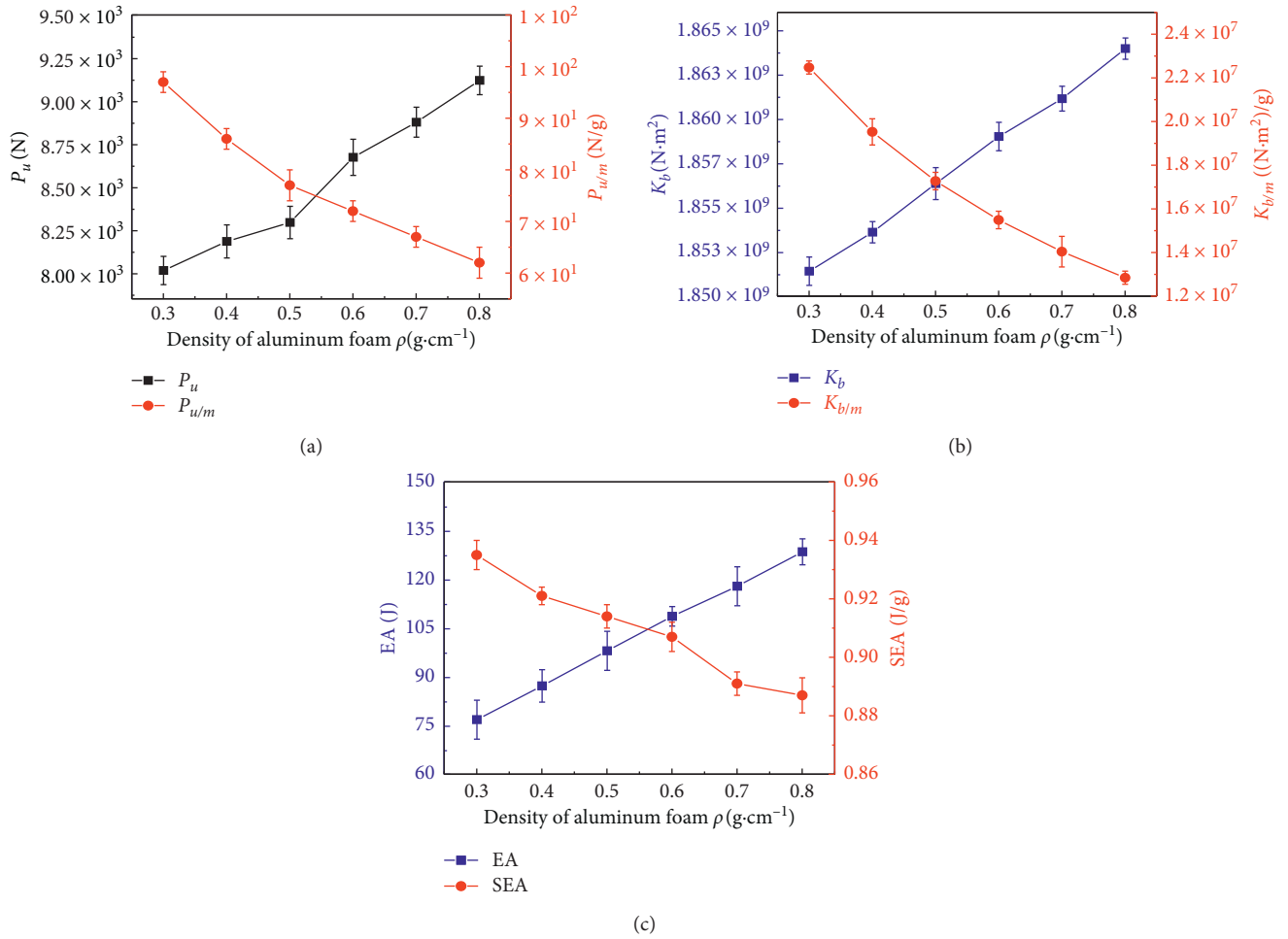

FIGURE 14: Mechanical properties of filled CFRP square tube changing with the density of aluminum foam: (a) ultimate load (P_u) and specific ultimate load ($P_{u/m}$), (b) bending stiffness (K_b) and specific bending stiffness ($K_{b/m}$), and (c) energy absorption (EA) and specific energy absorption (SEA).

density as the filler material can achieve greater benefits of lightweight.

6. Conclusion

In this paper, the aluminum foam filling effect for the bending behavior of CFRP square tubes was studied by combination of bending experiments, numerical model, and analytical method. The typical load-deflection histories, strain distribution, bending characteristics, and failure mechanisms of all the tested specimens were investigated. Within the limitation of the study, the important conclusions can be summarized as follows:

(1) The load-deflection curves of the aluminum foam, hollow CFRP square tube, and CFRP square tube filled with aluminum foam were divided into initial elastic bending stage and bending collapse stage. The full-field strain distributions of the experimental measurement and numerical prediction were well agreed. It is worth noting that aluminum foam as a lightweight filler material, because of the interaction between the bended walls of CFRP square tube and the internal aluminum foam, can significantly improve the load-carrying capacity of CFRP square tubes under bending load.

(2) The damage evolvement process and various failure modes of the CFRP square tube filled with aluminum foam were experimentally captured and numerically predicted, comparing to the aluminum foam and hollow tubes. Due to the aluminum foam filling effect, the filled tubes showed a more complex damage evolution process, including the indentation, buckling, plastic hinges, shear interaction, core failure, and bulging deformation.

(3) The experimental results showed a good agreement with the data calculated by the numerical model and analytical model, and the average errors were within 5%. Researches showed that the aluminum foam can improve the bending properties of the filled tubes under bending load, especially the load-carrying capacity and energy absorption characteristics.

Besides, with the increase of the aluminum foam density, the ultimate load, bending stiffness, and energy absorption of the filled tubes increased, while the specific ultimate load, specific bending stiffness, and specific energy absorption decreased. Therefore, the use of low-density aluminum foam as filler can achieve greater lightweight benefits.

Data Availability

The numerical and experimental data used to support the findings of this study are available from the corresponding author upon request.

Conflicts of Interest

The authors declare that they have no conflicts of interest.

References

[1] C.-K. Park, C.-D. Kan, and W. T. Hollowell, "Evaluation of crashworthiness of a carbon-fibre-reinforced polymer (CFRP) ladder frame in a body-on-frame vehicle," *International Journal of Crashworthiness*, vol. 19, no. 1, pp. 27–41, 2014.

[2] W. Wu, Q. Liu, Z. Zong, G. Sun, and Q. Li, "Experimental investigation into transverse crashworthiness of CFRP adhesively bonded joints in vehicle structure," *Composite Structures*, vol. 106, pp. 581–589, 2013.

[3] B. P. Bussadori, K. Schuffenhauer, and A. Scattina, "Modelling of CFRP crushing structures in explicit crash analysis," *Composites Part B: Engineering*, vol. 60, pp. 725–735, 2014.

[4] Q. Liu, O. Guo, Y. Ju, Y. Lin, and Q. Li, "Impact responses and residual flexural properties of narrow CFRP laminates," *Composite Structures*, vol. 111, pp. 332–339, 2014.

[5] M. Langseth and O. S. Hopperstad, "Static and dynamic axial crushing of square thin-walled aluminium extrusions," *International Journal of Impact Engineering*, vol. 18, no. 7-8, pp. 949–968, 1996.

[6] P. Feraboli and A. Masini, "Development of carbon/epoxy structural components for a high performance vehicle," *Composites Part B: Engineering*, vol. 35, no. 4, pp. 323–330, 2004.

[7] H. Ning, S. Pillay, and U. K. Vaidya, "Design and development of thermoplastic composite roof door for mass transit bus," *Materials & Design*, vol. 30, no. 4, pp. 983–991, 2009.

[8] P. Feraboli, A. Masini, L. Taraborrelli, and A. Pivetti, "Integrated development of CFRP structures for a topless high performance vehicle," *Composite Structures*, vol. 78, no. 4, pp. 495–506, 2007.

[9] Q. Liu, Y. Lin, Z. Zong, G. Sun, and Q. Li, "Lightweight design of carbon twill weave fabric composite body structure for electric vehicle," *Composite Structures*, vol. 97, pp. 231–238, 2013.

[10] X. Zhang and H. Zhang, "Energy absorption of multi-cell stub columns under axial compression," *Thin-Walled Structures*, vol. 68, pp. 156–163, 2013.

[11] Q. Liu, H. Xing, Y. Ju, Z. Ou, and Q. Li, "Quasi-static axial crushing and transverse bending of double hat shaped CFRP tubes," *Composite Structures*, vol. 117, pp. 1–11, 2014.

[12] Q. Liu, Z. Ou, Z. Mo, Q. Li, and D. Qu, "Experimental investigation into dynamic axial impact responses of double hat shaped CFRP tubes," *Composites Part B: Engineering*, vol. 79, pp. 494–504, 2015.

[13] X. Deng, W. Liu, and Z. Lin, "Experimental and theoretical study on crashworthiness of star-shaped tubes under axial compression," *Thin-Walled Structures*, vol. 130, pp. 321–331, 2018.

[14] A. G. Mamalis, D. E. Manolakos, M. B. Ioannidis, P. K. Kostazos, and C. Dimitriou, "Finite element simulation of the axial collapse of metallic thin-walled tubes with octagonal cross-section," *Thin-Walled Structures*, vol. 41, no. 10, pp. 891–900, 2003.

[15] A. Eyvazian, M. K. Habibi, A. M. Hamouda, and R. Hedayati, "Axial crushing behavior and energy absorption efficiency of corrugated tubes," *Materials & Design (1980–2015)*, vol. 54, pp. 1028–1038, 2014.

[16] H. Mozafari, A. Eyvazian, A. M. Hamouda, V. Crupi, G. Epasto, and E. Gugliemino, "Numerical and experimental investigation of corrugated tubes under lateral compression," *International Journal of Crashworthiness*, vol. 23, no. 4, pp. 461–473, 2018.

[17] K. Vinayagar and A. Senthil Kumar, "Crashworthiness analysis of double section bi-tubular thin-walled structures," *Thin-Walled Structures*, vol. 112, pp. 184–193, 2017.

[18] Z. Ahmad and D. P. Thambiratnam, "Dynamic computer simulation and energy absorption of foam-filled conical tubes under axial impact loading," *Composites Structures*, vol. 87, no. 3-4, pp. 186–197, 2009.

[19] R. D. Hussein, D. Ruan, and J. W. Yoon, "An experimental study of square aluminium tubes with honeycomb core subjected to quasi-static compressive loads," *Key Engineering Materials*, vol. 626, pp. 91–96, 2014.

[20] A. Ghamarian, H. R. Zarei, and M. T. Abadi, "Experimental and numerical crashworthiness investigation of empty and foam-filled end-capped conical tubes," *Thin-Walled Structures*, vol. 49, no. 10, pp. 1312–1319, 2011.

[21] J. S. Lin, X. Wang, and G. Lu, "Crushing characteristics of fiber reinforced conical tubes with foam-filler," *Composite Structures*, vol. 116, pp. 18–28, 2014.

[22] Q. Gong, H. Zhu, Z. G. Yan, B. Q. Huang, Y. Zhang, and D. Y. Dong, "Fracture and delamination assessment of prestressed composite concrete for use with pipe jacking method," *Mathematical Problems in Engineering*, vol. 2015, Article ID 579869, 11 pages, 2015.

[23] B. A. Danawade and R. R. Malagi, "Design and manufacturing of wood filled steel tubes for structural applications," *Materials Today: Proceedings*, vol. 18, pp. 4133–4142, 2019.

[24] X. Zhu, C. Xiong, J. Yin, D. Yin, and H. Deng, "Bending experiment and mechanical properties analysis of composite sandwich laminated box beams," *Materials*, vol. 12, no. 18, p. 2959, 2019.

[25] N. Movahedi and E. Linul, "Quasi-static compressive behavior of the ex-situ aluminum-alloy foam-filled tubes under elevated temperature conditions," *Materials Letters*, vol. 206, pp. 182–184, 2017.

[26] S. Mohsenizadeh and Z. Ahmad, "Auxeticity effect on crushing characteristics of auxetic foam-filled square tubes under axial loading," *Thin-Walled Structures*, vol. 145, Article ID 106379, 2019.

[27] S. Asavavisithchai, D. Slater, and A. R. Kennedy, "Effect of tube length on the bucking mode and energy absorption of Al foam-filled tubes," *Journal of Materials Science*, vol. 39, no. 24, pp. 7395-7396, 2004.

[28] T. Fiedler, K. Al-Sahlani, P. A. Linul, and E. Linul, "Mechanical properties of A356 and ZA27 metallic syntactic foams at cryogenic temperature," *Journal of Alloys and Compounds*, vol. 813, Article ID 152181, 2020.

[29] S. Shi, Z. Sun, X. Hu, and H. Chen, "Flexural strength and energy absorption of carbon-fiber-aluminum-honeycomb composite sandwich reinforced by aluminum grid," *Thin-Walled Structures*, vol. 84, pp. 416–422, 2014.

[30] X. Huang, C. Yin, J. Huang et al., "Hypervelocity impact of TiB_2-based composites as front bumpers for space shield applications," *Materials & Design*, vol. 97, pp. 473–482, 2016.

[31] C. C. Chiang, L. Tsai, and V. V. Thuyet, "Damage monitoring and analysis of the structure effect on strength of composite laminates," *Mathematical Problems in Engineering*, vol. 2015, Article ID 964062, 7 pages, 2015.

[32] A. G. Mamalis, D. E. Manolakos, M. B. Ioannidis, and D. P. Papapostolou, "Crashworthy characteristics of axially statically compressed thin-walled square CFRP composite tubes: experimental," *Composite Structures*, vol. 63, no. 3-4, pp. 347–360, 2004.

[33] A. Othman, S. Abdullah, A. K. Ariffin, and N. A. N. Mohamed, "Investigating the crushing behavior of quasi-static oblique loading on polymeric foam filled pultruded composite square tubes," *Composites Part B: Engineering*, vol. 95, pp. 493–514, 2016.

[34] Q. Liu, Z. Mo, Y. Wu, J. Ma, G. C. Pong Tsui, and D. Hui, "Crush response of CFRP square tube filled with aluminum honeycomb," *Composites Part B: Engineering*, vol. 98, pp. 406–414, 2016.

[35] G. Sun, S. Li, Q. Liu, G. Li, and Q. Li, "Experimental study on crashworthiness of empty/aluminum foam/honeycomb-filled CFRP tubes," *Composite Structures*, vol. 152, pp. 969–993, 2016.

[36] S. P. Mai, N. A. Fleck, and T. J. Lu, "Optimal design of box-section sandwich beams in three-point bending," *International Journal of Solids and Structures*, vol. 44, no. 14-15, pp. 4742–4769, 2007.

[37] T. P. Vo and J. Lee, "Flexural-torsional behavior of thin-walled composite box beams using shear-deformable beam theory," *Engineering Structures*, vol. 30, no. 7, pp. 1958–1968, 2008.

[38] T. P. Vo and J. Lee, "Flexural-torsional buckling of thin-walled composite box beams," *Thin-Walled Structures*, vol. 45, no. 9, pp. 790–798, 2007.

[39] T. P. Vo and J. Lee, "Flexural-torsional behavior of thin-walled closed-section composite box beams," *Engineering Structures*, vol. 29, no. 8, pp. 1774–1782, 2007.

[40] M. I. Geuchy and S. V. Hoa, "Flexural stiffness of thick walled composite tubes," *Composites Structures*, vol. 149, pp. 125–133, 2016.

[41] F. Shadmehri, B. Derisi, and S. V. Hoa, "On bending stiffness of composite tubes," *Composite Structures*, vol. 93, no. 9, pp. 2173–2179, 2011.

[42] N. Onsalung, C. Thinvongpi, and K. Painthong, "The influence of foam density on specific energy absorption of rectangular steel tubes," *Energy Research Journal*, vol. 1, no. 2, pp. 135–140, 2010.

[43] Y. Zhai, D. Li, X. Li, L. Wang, and Y. Yin, "An experimental study on the effect of bolt-hole clearance and bolt torque on single-lap, countersunk composite joints," *Composite Structures*, vol. 127, pp. 411–419, 2015.

[44] J. Hu, K. Zhang, Q. Yang, H. Cheng, P. Liu, and Y. Yang, "An experimental study on mechanical response of single-lap bolted CFRP composite interference-fit joints," *Composite Structures*, vol. 196, pp. 76–88, 2018.

[45] Z. Hashin, "Failure criteria for unidirectional fiber composites," *Journal of Applied Mechanics*, vol. 47, no. 2, pp. 329–334, 1980.

[46] Z. Hashin and A. Rotem, "A fatigue failure criterion for fiber reinforced materials," *Journal of Composite Materials*, vol. 7, no. 4, pp. 448–464, 1973.

[47] P. W. Harper and S. R. Hallett, "Cohesive zone length in numerical simulations of composite delamination," *Engineering Fracture Mechanics*, vol. 75, no. 16, pp. 4774–4792, 2008.

[48] Q. Liu and G. Subhash, "A phenomenological constitutive model for foams under large deformations," *Polymer Engineering and Science*, vol. 44, no. 3, pp. 463–473, 2004.

[49] S. Jose, R. Ramesh Kumar, M. K. Jana, and G. Venkateswara Rao, "Intralaminar fracture toughness of a cross-ply laminate and its constituent sub-laminates," *Composites Science and Technology*, vol. 61, no. 8, pp. 1115–1122, 2001.

[50] M. L. Benzeggagh and M. Kenane, "Measurement of mixed-mode delamination fracture toughness of unidirectional glass/epoxy composites with mixed-mode bending apparatus," *Composites Science and Technology*, vol. 56, no. 4, pp. 439–449, 1996.

[51] H. Cui, Q. Yan, X. M. Wang, S. Q. Bi, and X. F. Wang, "Assessment of failure analysis method for the bolted structure between selective laser melting aluminum plate and CFRP composite laminate," *Acta Material Compositae Sinica*, vol. 34, no. 12, pp. 2762–2769, 2017.

[52] I. Duarte, M. Vesenjak, L. Krstulović-Opara, I. Anžel, and J. M. F. Ferreira, "Manufacturing and bending behaviour of in situ foam-filled aluminium alloy tubes," *Materials & Design*, vol. 66, pp. 532–544, 2015.

[53] Q. Liu, X. Xu, J. Ma, J. Wang, Y. Shi, and D. Hui, "Lateral crushing and bending responses of CFRP square tube filled with aluminum honeycomb," *Composites Part B: Engineering*, vol. 118, pp. 104–115, 2017.

[54] M. H. Shojaeifard, H. R. Zarei, R. Talebitooti, and M. Mehdikhanlo, "Bending behavior of empty and foam-filled aluminum tubes with different cross-sections," *Acta Mechanica Solida Sinica*, vol. 25, no. 6, pp. 616–626, 2012.